GEOMETRIC AND RADIOMETRIC INVESTIGATIONS OF CARTOSAT-1 DATA

E. Baltsavias*, S. Kocaman, D. Akca, K. Wolff

Institute of Geodesy and Photogrammetry, ETH Zurich
Wolfgang-Pauli-Str. 15, CH-8093 Zurich, Switzerland – (manos, skocaman, akca, wolff@geod.baug.ethz.ch)

KEY WORDS: Cartosat-1, image quality, image preprocessing, sensor modelling, RPCs, 3D point positioning, DSM generation, performance evaluation

ABSTRACT:
The Institute of Geodesy and Photogrammetry (IGP) is participating in the Cartosat-1 evaluation program, a common initiative of ISRO (India) and ISPRS. Within this program various test sites with reference data have been established and Cartosat-1 images have been acquired over these sites. Here, we will report about our investigations at the Rome and Mausanne test sites. First, we report on radiometric problems encountered with the images and preprocessing for their improvement. These include artefacts, unfocussing in the forward channel and scale differences to aft, jitter at horizontal edges, interlacing errors and pattern noise. We show examples and also preprocessing methods that can be employed in order to improve image quality, with aim especially to automatically generate a DSM with less blunders (due to noise and artefacts) and more match points. Then, we report on sensor modelling and the 3D point positioning accuracy that can be achieved, as well as various problems encountered with the Rational Polynomial Coefficients (RPCs). The orientation results were produced using various options regarding image preprocessing, sensor model, number and distribution of GCPs and GCP image mensuration methods. The best results led to a planimetric and height accuracy (RMSE) of about 1.3 m. The absolute geolocation accuracy varies greatly from dataset to dataset and can be worse than a few thousand meters, making Cartosat-1 unsuitable for generation of global mapping products without use of GCPs. Finally, we present the results of automatic DSM generation using our own Sat-PP program package. Various DSMs were generated with 10m grid spacing. The results were checked both visually and were compared using the provided reference data. In the best case, the achieved accuracy is about 2.7 m without any manual editing and in spite of 3-year difference between matching and reference DSM. In spite of several aspects that could and should be improved, Cartosat-1 is a useful sensor for mapping and especially generation of DSMs.

1. INTRODUCTION

High spatial resolution optical satellite sensors have been subject of scientific investigations and evaluations since 2000. Some of them provide a ground sampling distance (GSD) of 1m or less but each image covers a small area, their price is high, and stereo coverage is often rare. Thus, the last years some sensors have been launched with a GSD of 2.5 – 5 m, covering a much larger area per image, having much lower image price and tailored to acquisition of stereo images and derivation of DSMs by using 2- or 3-line CCDs. Typical examples include Spot-5 HRG, Alos Prism and Cartosat-1. Such systems are suitable also for derivation of global DSMs, if the absolute geolocation accuracy of the images is good enough (e.g. Spot-5).

The investigations in this paper are part of the ISPRS-ISRO Cartosat-1 Scientific Assessment Programme (C-SAP). IGP acts as principal investigator for some test sites and has evaluated data from other test sites. Here, we will report on our investigations with the Rome and Mausanne test sites. Results at these test sites have been reported previously by other groups: e.g. for Rome (Crespi et al., 2006; Sadasiva Rao et al., 2006) and for Mausanne (Kay and Zielinski, 2006; Lehner et al., 2006; Jakobsen, 2006). These reports can be used as a comparison to the results we report below.

A description of the Cartosat-1 mission is given in EOPortal (2007) and Krishnaswamy (2002). Here, we remind some of the parameters, that are relevant for the discussion below. Cartosat-1 has a forward (F) and aft (A) panchromatic camera for along-track stereo, with a tilt in flight direction of +26° and -5 °, respectively. Each sensor is comprised of 12,000 pixels with 7 microns pixel spacing. According to ISRO, the sensor consists of two staggered line CCDs (however if the staggering aims at increase of GSD, each staggered CCD should have 6000 pixels and 14 microns pixel spacing). Identical images of the two staggered CCDs are taken with a time difference of about 1.7 ms. Orientation instabilities during this period, may cause problems when synthesizing the final image from the images of the two staggered CCDs. The CCDs are not of TDI technology and the integration time is 0.336 ms. The base to height (B/H) ratio is about 0.62. Data are quantized with 10-bit and compressed by a factor of 3.22, with little image quality losses. The nominal GSD is 2.2-2.5 m, and the typical image size is 12,000 x 12,000 pixels. The image scale is about 1:312,000. The geolocation accuracy of the images, as given by ISRO, (without GCPs, 3 sigma) is 250 m (design) and 150 m (achieved). The satellite has a yaw steering, except over India, in order to compensate the Earth rotation effect or acquire a wider mono strip. A pitch bias is also possible to acquire occluded areas in case of large slopes along track. A roll bias allows across-track pointing. Dynamic changes, especially the yaw steering and pitch bias may affect both geometric stability and radiometric quality.

2. INPUT DATA

The test data of Rome are described in Crespi et al. (2006) and of Mausanne in Kay and Zielinski (2006) and Spruyt and Kay (2004). In both cases, the images were of the Standard, Orthokit product type and were delivered with RPCs. It should be noted that the Rome images were acquired on June 8th 2005 only about one month after launch, posing questions about their quality, since one month is usually not sufficient for the calibration and validation phase of a satellite sensor. The Mausanne images processed were of January 31st, 2006. The initial Rome dataset (called Rome_Old) had very poor GCPs.

* Corresponding author.

The quality of GCP definition was medium to unacceptable. They were collected for Eros 1A images, and were not selected based on whether they were well identifiable in the Cartosat-1 images or not, and included small objects hardly visible in the images. In fact, some of them were practically invisible. Many GCPs were outside the images. The distribution of the GCPs in N-S was very poor covering only 2,500 pixels out of the 12,000 (one GCP only was 450 pixel further south). Due to these serious problems, this dataset should not have been accepted and distributed by the C-SAP team. Thus, some GCPs were omitted in the further computations due to the very poor definition, and 2 could not be found. The reference height data were also inappropriate. They consisted of vectors of digital maps describing the terrain. At a later stage, we received from the principal investigator (PI) for Rome (Università di Roma "La Sapienza") new reference data, not distributed via the C-SAP team. The GCPs were covering more or less the whole image and were measured on ground with GPS (5 cm accuracy) and in the images manually using PCI Geomatica. About half of the points were part of the old GCPs, the rest were new. The reference data included a 0.5 m grid DSM derived from aerial images (2 strips with 6 images each, 1:9000 scale, 14 cm GSD, taken in June 2004 - almost exactly one year before the Cartosat-1 images) which was generated using the program Sat-PP (see section 5). The DSM however covered only a very small region of the Cartosat-1 images, about 2.5 x 5 km, with flat terrain, buildings, vegetation, and some open areas. The DSM gave orthometric heights, while our derived matching DSM was in WGS84, however the offset between the two height datums was corrected. We call this dataset Rome_New. The Mausanne dataset was by far superior. In fact, at least until the ISPRS Commission IV in Goa, September 2006, this was, in our opinion, the only dataset that included accurate, well distributed GCPs and accurate reference DSMs. For these reasons, the conclusions drawn from our investigations should rely more on the Mausanne than the Rome dataset. The original reference DSM in Mausanne that was distributed by C-SAP was actually a less accurate DTM, produced by filtering of the DSM, both produced by ISTAR. Thus, we requested from JRC the original 2m grid DSM for comparison. It was generated from ADS40 images with a GSD of 0.5 m through matching and some manual editing, with a declared RMS accuracy of 34 cm using 33 GPS check points. Unfortunately, for reasons unknown to us, Istar delivered to JRC approximately only half of the area where a DSM had been generated. This was however large enough, with variable terrain relief (flat, hilly) and landcover, including various types of agricultural areas (trees, bushes, arable fields, some with low texture and often repetitive patterns). 13 GCPs came from GPS measurements (with accuracy 5 and 10 cm for planimetry and height) and another 18 from true orthoimages, generated with the reference DSM (with accuracy 43 and 34 cm for planimetry and height). All GCPs were measured in the images manually. Their identification in the images was not easy, especially in such an agricultural area, with lack of many anthropogenic objects. Although the second GCP group from the orthoimages was expected to be less accurate, with the Cartosat-1 GSD and the difficulties in identifying the GCPs in the images, even the second group is fully sufficient. This was also verified by the sensor orientation tests (Tables 4 and 5), where the residuals of the second group were similar to the first one in X and Z, and only slightly worse in Y.

All processing was performed with the delivered RPCs (called old RPCs). However, during matching, as explained in section 5, numerical instabilities of the RPCs due to zero crossings in the denominator were observed leading to huge numbers for the object coordinates. Thus, we requested from ISRO new RPCs without zero crossings, based on a new, modified method for their computation. The new RPCs were used with the same old images, assuming that for the generation of the Orthokit products, the strict sensor model was used and not the RPCs.

3. IMAGE QUALITY AND PREPROCESSING

Regarding image quality, the following can be observed. First, the dynamic range of the images after a Gaussian-type mapping to 8-bits was examined. For the Mausanne images, the significant grey levels were 55-60 for A and 60 for F. For Rome images, these values were 190 and 155 respectively, due to the much higher sun elevation. There are no noticeable artefacts due to compression. The F channel is much less sharp than the A (looks like defocused). Both channels exhibit pattern noise and differences between even and odd columns (interlacing). This is more obvious in the A channel because it is sharper. There is a certain degree of saturation, especially in the Rome images, that include an urban area with a significant number of specularly reflecting objects and buildings which often appear bright in satellite images. This was partly also due to the higher sun elevation, which was actually almost the opposite of the F elevation. Horizontal (but not vertical) edges exhibit a jitter especially in the F channel, i.e. there is a vertical shift of the edge between odd and even columns. This is possibly due to a suboptimal method of generating the image from the 2 staggered CCDs or high-frequency pitch instabilities that have a larger influence on the F channel. The images look cluttered, and there is no nice definition of object outlines (partly also due to the 2.5 m GSD). In the Rome images, some artefacts were observed, i.e. about every 1000 rows, along the whole image width, as short (5 pixel) vertical bright lines every second column. Although the images are taken quasi simultaneously, there are many locations with large radiometric differences between A and F, especially in the Rome images. This creates problems for matching and leads to blunders. A possible reason for this may be the selection of the tilts for the A and F channels. We believe that these differences would be reduced for an Aft, Backward configuration, or a symmetric Aft Backward configuration around the nadir (for the Northern Hemisphere). The Mausanne images due to their smaller contrast exhibited almost no saturation, less radiometric differences between A and F, and less pattern noise. Also no artefacts were observed. The remaining problems were as with the Rome images. A factor that also influences image quality is the lack of TDI and the relatively short integration time. Several of these radiometric problems are shown in Figs. 1 and 2.

We tried to improve the image quality through preprocessing. This is not so important for GCP measurement, especially a manual one, but it is very important for matching. For the Rome images, we first reduced the 10- to 8-bit using a Gaussian-type mapdown. Then, the interlacing was reduced by an own algorithm. The artefacts were reduced by using a destriping function of Photoshop. However, its performance was not very good. Then, an adaptive edge enhancing noise reduction was performed. For the high clutter and pattern noise of Cartosat-1 images, this unfortunately led to an enhancement of small area noise, especially after a subsequent Wallis filtering for contrast enhancement and radiometric equalisation. This led to a salt and pepper noise, which was reduced by a 3x3 median. This preprocessing (called preprocessing 1) was applied for the Rome images.

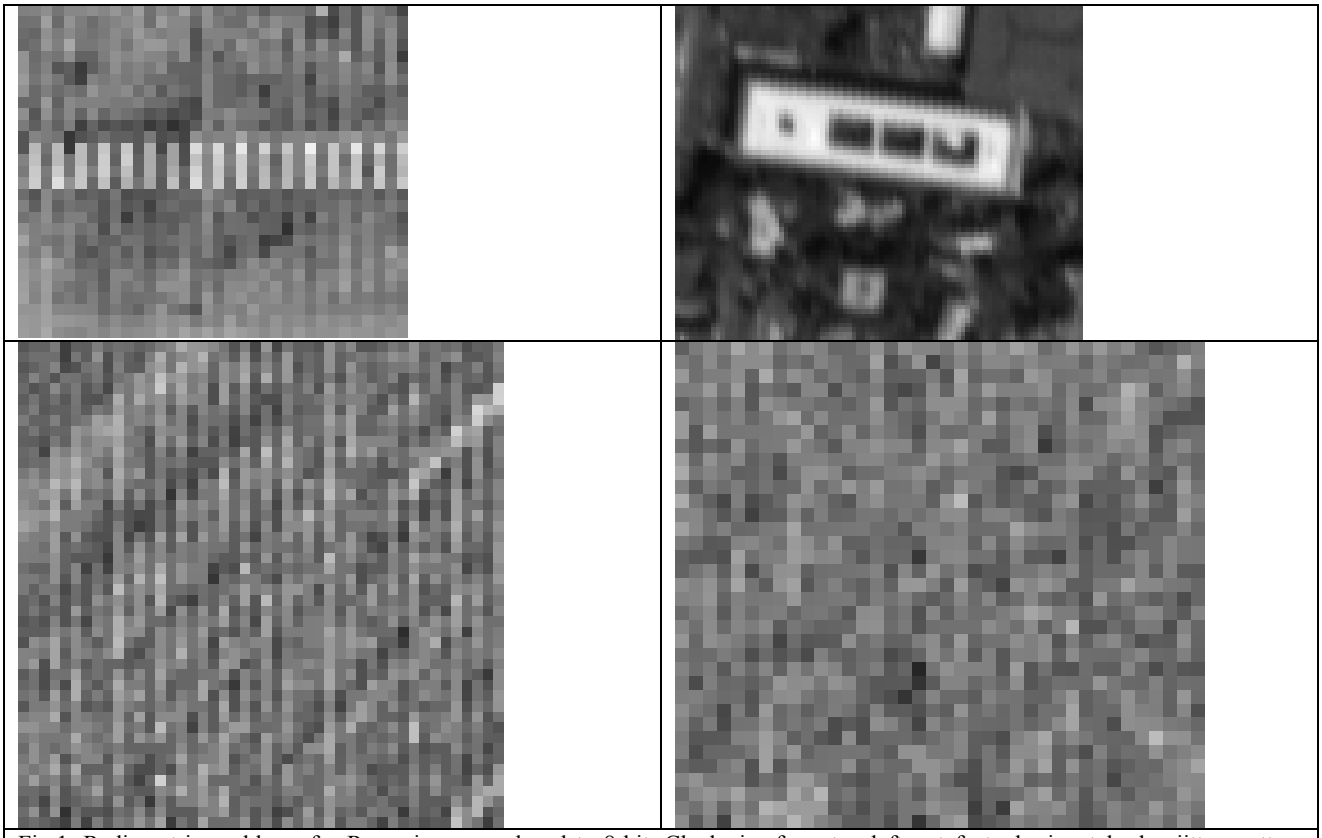

Fig.1. Radiometric problems for Rome images reduced to 8-bit. Clockwise from top left: artefacts, horizontal edge jitter, pattern noise, interlacing. The two last problems overlap each other. All examples are for A after a Wallis filtering to enhance visualistion. The edge jitter is for F, without Wallis.

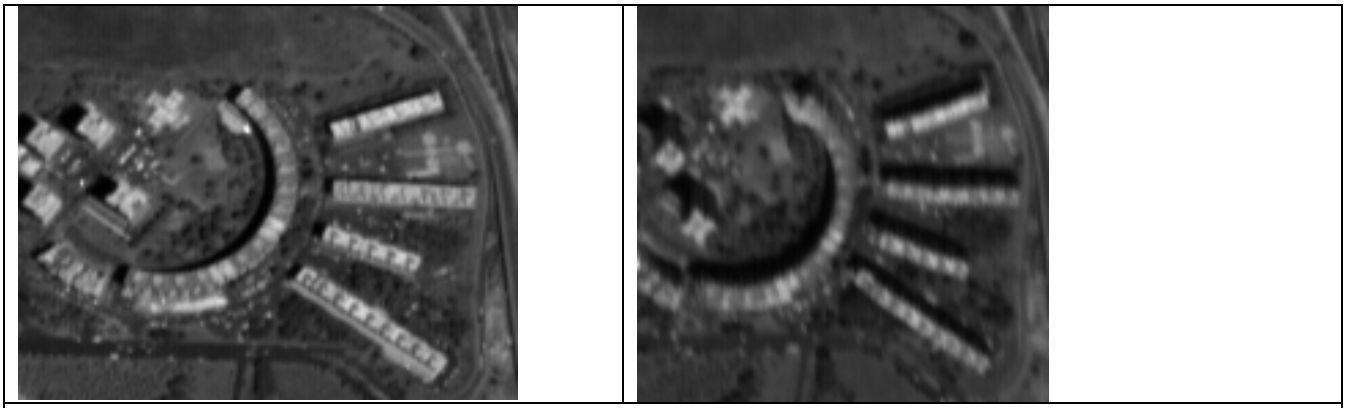

Fig. 2. Sharpness and scale differences and radiometric differences due to shadows, occlusions and different sensor to illumination angle between A (left) and F (right) of Rome images. Other interesting examples of differences between A and F are shown in Lutes (2006).

It led to a reduction of the contrast in very low texture areas. Thus, the grid and interest points used in matching (see section 5) were less. However, the edge match points were increased a lot, thus leading to a better DSM. The many preprocessing steps may have altered a bit, the edge geometry, which would be a problem for the measurement of the GCPs by least squares matching (see section 4). However, we do not think that this has happened, based on the relatively good results of the sensor orientation (see Table 3). For the Mausanne images, we simplified the preprocessing (preprocessing 2). The same 10- to 8-bit reduction was applied, then a Wallis filter, and finally a 3x3 Gaussian filter. The de-interlacing filter was not applied due to time constraints. A comparison of Rome and Mausanne images, before and after preprocessing, for the 8-bit reduced images is shown in Figs. 3 and 4.

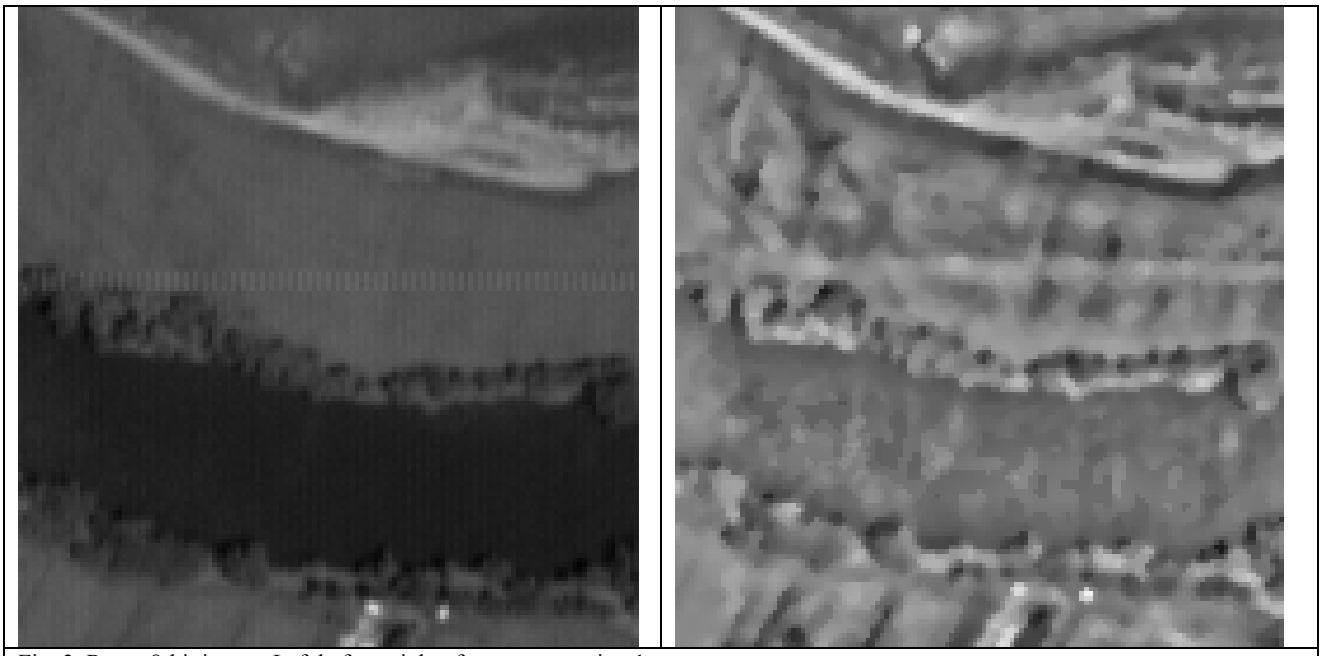

Fig. 3. Rome 8-bit image. Left before, right after preprocessing 1.

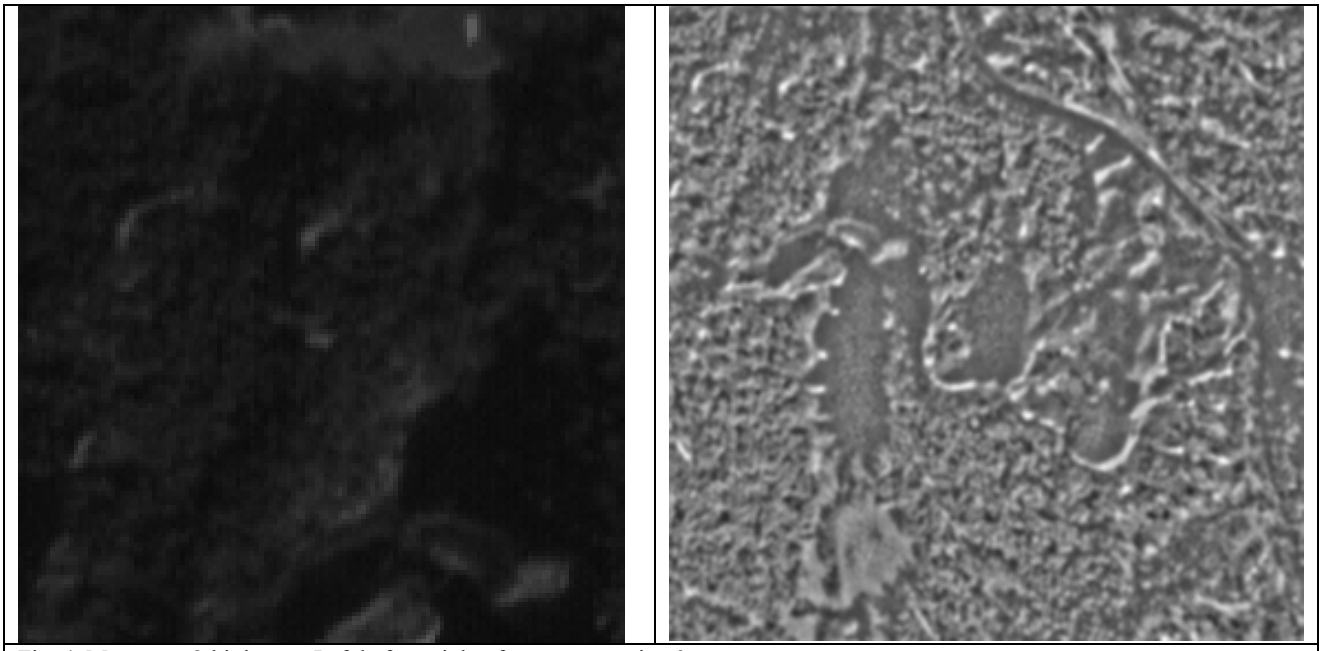

Fig. 4. Mausanne 8-bit image. Left before, right after preprocessing 2.

4. SENSOR ORIENTATION AND ACCURACY OF 3D POINT MEASUREMENT

The measurement of GCPs in the images was performed as follows. For Rome_Old we used provided sketches (often with little relation to the image content) to identify the points in the A image. The points in the F image were measured manually, and also by least squares matching (LSM), using an affine or conformal transformation, using the points in the A image as template. The latter method was used with 2 types of preprocessing: a) no preprocessing, just a reduction to 8-bit, and b) the preprocessing mentioned in section 3. This was not done for the manual measurements, because in this case preprocessing is not so important, as the human eye can tolerate a significant amount of noise. For the Mausanne data we used: a) the pixel coordinates as provided by the principal investigator (JRC), and b) the points in the A image as they were delivered and transferring them in the F image by LSM. LSM reduces the parallax errors between corresponding points and this leads to an improvement of the height accuracy (the planimetric accuracy can still have problems, if the identification of the point in the A image is wrong). It was interesting to note, than the F had in the affine transformation of LSM a consistent y-shear with respect to A.

As sensor model, we used RPCs and then a correction by two shifts (RPC1), RPCs and then a correction by an affine transformation (RPC2) and a 3D-affine transformation (3DAFF). Regarding the control point selection we used three variants: a) all points as GCPs (version ALL), b) 6 well

distributed GCPs (version 6), and c) 6 poorly distributed GCPs, covering about 1/3 of the image area in each image dimension (version 6B). This permits to check the influence of the number and distribution of the control points on the results. The results for Rome_Old are given here, due to lack of space, only for the LSM measurement, using the preprocessed images (see Table 1). The results with LSM and non-preprocessed images were very similar, while those with manual measurements were less accurate in Z.

Table 1. Results of sensor orientation for Rome_Old dataset (CPs = check points). The RMS values are given for both CPs and GCPs.

Orientation version	**No. of GCPs**	**No. of CPs**	**Sigma-0 (pixels)**	**RMSE-X (m)**	**RMSE-Y (m)**	**RMSE-Z (m)**
RPC1	ALL (32)	0	1.73	5.3	2.1	3.5
RPC2	ALL (32)	0	0.82	1.8	1.8	2.6
3DAFF	ALL (32)	0	0.85	1.8	1.8	2.4
RPC1	6	26	1.34	5.6	2.1	3.5
RPC2	6	26	0.42	1.9	1.8	2.8
3DAFF	6	26	0.42	2.3	2.6	2.8
RPC1	6B	26	0.75	5.3	2.1	3.6
RPC2	6B	26	0.51	2.2	1.9	2.65
3DAFF	6B	26	0.52	2.2	1.9	3.0

The best results were with RPC2 and all GCPs, giving an RMSE of 0.7 pixel in X and Y and 1 pixel in Z. The sigma-0 values fit well with the RMSE when all GCPs are used, otherwise they are quite optimistic. The RPC1 versions were clearly less accurate (especially in X and secondary in Z), showing that Cartosat-1 needs, compared to Ikonos, higher order terms to model the imaging geometry. The 3D affine transformation is generally sensitive to terrain height range, number and distribution of GCPs. In this dataset, the area extent was small, and the height range small, so there was no big difference between RPC2 and 3DAFF. However 3DAFF starts showing a deterioration with 6B, where the GCP distribution was poor. The accuracy deterioration when using only 6 instead of all GCPs is small. The same applies to the change of the distribution of the GCPs (compare versions 6 and 6B).

The results for the Rome_New datasets are shown in Tables 2 and 3 for the image coordinates as delivered by the PI and after LSM respectively. These results are more reliable than those of Table 1 due to the larger number of GCPs, their better quality and better distribution. However, the conclusions are very similar to the ones of Table 1. With the exception that for the versions 6B there is a noticeable increase of RMS-X compared to the versions 6, showing that there is indeed a sensitivity to the GCP distribution. Table 3 compared to Table 2 shows that with image coordinates measured by LSM the height accuracy improves. The best values of Table 3 with RPC2 and all GCPs correspond to 0.55 pixels in X and Y and 0.7 pixels in Z, a result which is quite acceptable.

Table 2. Results of sensor orientation for Rome_New dataset and image coordinates as provided by the PI (CPs = check points). The RMS values are given for both CPs and GCPs.

Orientation version	**No. of GCPs**	**No. of CPs**	**RMSE-X (m)**	**RMSE-Y (m)**	**RMSE-Z (m)**
RPC1	ALL (42)	0	5.1	1.9	2.7
RPC2	ALL (42)	0	1.5	1.5	2.2
3DAFF	ALL (42)	0	1.4	1.3	2.2
RPC1	6	36	5.1	2.1	2.8
RPC2	6	36	1.7	1.8	2.4
3DAFF	6	36	1.5	1.6	2.3
RPC1	6B	36	5.8	2.6	3.1
RPC2	6B	36	2.7	1.5	2.0
3DAFF	6B	36	1.9	1.6	3.1

Table 3. Results of sensor orientation for Rome_New dataset and image coordinates from LSM (CPs = check points). The RMS values are given for both CPs and GCPs.

Orientation version	**No. of GCPs**	**No. of CPs**	**RMSE-X (m)**	**RMSE-Y (m)**	**RMSE-Z (m)**
RPC1	ALL (42)	0	5.0	1.9	2.4
RPC2	ALL (42)	0	1.3	1.4	1.8
3DAFF	ALL (42)	0	1.3	1.4	1.8
RPC1	6	36	5.0	2.0	2.7
RPC2	6	36	1.5	1.6	2.1
3DAFF	6	36	1.4	1.6	2.1
RPC1	6B	36	5.7	2.1	2.6
RPC2	6B	36	2.7	1.5	2.0
3DAFF	6B	36	1.9	1.6	3.1

The results for Mausanne are shown in Tables 4 and 5, for the image coordinates as delivered by the PI and after LSM respectively. The results of Mausanne are more reliable than those of Rome due to the better quality of the GCPs, the much larger image width of 12,000 pixels compared to the 3000 pixels of Rome images and the fact that the terrain relief was more variable with larger height range. The image dimensions and the terrain relief influenced a lot the performance of the 3DAFF, which as shown in Tables 4 and 5 leads to unacceptable results for all orientation versions, while the object coordinate residuals show very clear systematic trends. The difference between RPC1 and RPC2 is as for the Rome data. To analyse the role of GCP number and distribution, only the RPC2 versions should be considered. Version 6 compared to version ALL shows a slight deterioration in Y, and more in Z, which can not be ignored. Comparing versions 6B and 6, shows that a poor distribution leads to a deterioration in Y, and for Table 4 also in Z. Summarising, the Cartosat-1 is not that insensitive to number and especially distribution of GCPs as other sensors like Ikonos. A comparison of the RPC2 versions between Tables 4 and 5 shows a significant improvement in Z when measuring with LSM. The best results of Table 5, correspond to an accuracy in X, Y and Z of 0.6, 0.7 and 0.5 pixels. While this planimetric accuracy is inferior to the one achieved with Ikonos and Quickbird, the accuracy is high in height, even more if one considers the suboptimal B/H ratio.

All above results were with the old RPCs. The new RPCs led to very similar results. Obviously, the instability of the old RPCs influences only very few, random pixels, and this was not the case with our GCPs.

Table 4. Results of sensor orientation for Mausanne dataset and image coordinates as provided by the PI (CPs = check points). The RMS values are given for both CPs and GCPs.

Orientation version	**No. of GCPs**	**No. of CPs**	**RMSE-X (m)**	**RMSE-Y (m)**	**RMSE-Z (m)**
RPC1	ALL (31)	0	5.6	2.7	6.6
RPC2	ALL (31)	0	1.8	1.8	2.6
3DAFF	ALL (31)	0	28.6	7.3	17.1
RPC1	6	25	5.6	2.7	7.7
RPC2	6	25	1.8	2.0	3.3
3DAFF	6	25	30.9	14.9	19.9
RPC1	6B	25	5.7	3.0	6.6
RPC2	6B	25	2.1	3.2	5.3
3DAFF	6B	25	37.0	11.4	22.5

Table 5. Results of sensor orientation for Mausanne dataset and image coordinates from LSM (CPs = check points). The RMS values are given for both CPs and GCPs.

Orientation version	**No. of GCPs**	**No. of CPs**	**RMSE-X (m)**	**RMSE-Y (m)**	**RMSE-Z (m)**
RPC1	ALL (31)	0	5.5	2.8	6.0
RPC2	ALL (31)	0	1.4	1.8	1.3
3DAFF	ALL (31)	0	28.3	7.3	15.2
RPC1	6	25	5.6	2.8	6.9
RPC2	6	25	1.5	2.0	2.0
3DAFF	6	25	32	14.1	17.6
RPC1	6B	25	5.6	3.0	6.0
RPC2	6B	25	1.9	3.5	2.1
3DAFF	6B	25	39.9	12.2	21.7

We also examined plots for the object residuals. For RPC1 there was a clear systematic contraction in X. For RPC2 the residuals were random, while for 3DAFF they were very systematic in X direction. However, with RPC2 and 6B (but not version 6) the residuals were systematic showing a clear shearing in the Y direction, one more reason to avoid a suboptimal GCP distribution with Cartosat-1.

Another point of investigations was the examination of the old and new RPCs and their respective affine corrections for the Mausanne data. In the new RPCs, the values of the denominator coefficients were significantly smaller. In the numerator, the first 4 terms changed only slightly, while for higher terms the new coefficients were significantly smaller. While latitude, longitude and height scale and offset did not practically change, the line and sample offset and sample scale were substantially different. With different RPCs, it was expected than the affine corrections will also differ. The differences were not large with the exception of the F channel and the scale in x-direction, which almost doubled and changed sign. A comparison between A and F with the new RPCs showed significant differences in the scales. In both channels, the y-shift is much larger (2200-2300 pixels for Mausanne) than the x-shift (500-700 pixels for Mausanne), while the x-scale is about double the y-scale. When using the RPC1 model, the two shifts of the affine transformation do not change substantially. This means that by using only the RPCs, the absolute positioning accuracy corresponds to these two shifts, which in object space translate to 5500- 5750 m in Y and 1250-1750 m in X. For the Rome data, the shifts (absolute geolocation accuracy) were 200-830 m in Y, and 60-350 m in X, being larger for the F channel. These values are very different and much larger than the nominal absolute geolocation accuracy, especially for Mausanne, while they vary a lot from dataset to dataset. Some very useful insights in the Cartosat-1 RPCs and the 3D geopositioning accuracy are given by Lutes (2006).

5. DSM GENERATION AND ACCURACY ANALYSIS

After orientation, the best result of each dataset was selected to be used for DSM generation. This was the use of RPCs with subsequent affine transformation, whereby all available ground points were used as control points. For matching, we used an algorithm and the respective program package Sat-PP developed at IGP which has been used extensively for various platforms, sensors and image scales (including various high-resolution satellite sensors) with very good results. Details of this matching method can be found in Zhang (2005) and examples of its use for matching of high-resolution satellite images in Poli et al. (2004), Baltsavias et al. (2006) and Wolff and Gruen (2007). The only important points for this test regarding the matching method and Sat-PP are the following. Sat-PP uses initially a modified cross-correlation (CC) and optionally at the final matching stage LSM, that improves a bit the accuracy, but mainly helps detecting additional blunders. The main advantage of Sat-PP when matching stereo images is that it matches very densely, with three different match-point primitives (regular image grid points, interest points, and edgels, listed here with increasing degree of accuracy). It does also a pretty good job in detecting large blunders, especially when LSM is used. In the Rome_Old data, only CC was used, for the rest, CC and LSM.

After matching with the Rome_Old dataset, we observed in the 3D coordinates of the matched points huge errors. In the Rome_New and Mausanne datasets the errors became even larger leading to a crash of the programme. This occurred even in cases when one point (pixel) had reasonable pixel coordinates in the images where it was measured and the immediate neighbouring pixels had correct object coordinates. We had never observed such a problem although the matching program has been used very extensively for years with various datasets and it was very difficult to believe that this was due to a software bug. We believed that this was due to numerical instabilities of the RPCs which for the case of Cartosat-1 have zero crossing in the denominator. This was already reported by Lutes (2006) and also Lehner et al. (2006) reported residuals in the order of km using the original RPCs. However, this problem of zero-crossings was never officially reported by ISRO and the participants of the C-SAP were not supplied with new RPCs, although accordings to statements of ISRO, RPCs without zero-crossings could be generated. After requests to ISRO, we received new RPCs and this problem was not observed any more, verifying that our assumption was true.

The result of Sat-PP matching is a regular grid. We select the grid spacing as 4 times the GSD (corresponding to the average point distance of the irregularly distributed raw match points), i.e. for Cartosat-1 10 m. A finer grid spacing, although possible, leads to a noisier DSM. The results of matching were analysed both quantitatively and qualitatively. For the Rome datasets, the reference DSM was covering only a small area, and secondly the orientation was not so accurate as in Mausanne. Thus, these results are a) not so representative and b) do not show the potential of Cartosat-1 regarding DSM generation. A visual inspection of just the matching DSM showed that at various locations there were blunders, e.g. in the order of 40-80 m, either positive or negative. Sat-PP can detect and exclude large blunders quite efficiently, however smaller blunders remain often undetected. These blunders were due a) to matching errors where texture was poor, fact that was made worse by the image noise, b) places where due to the image artefacts mentioned above and in spite of the preprocessing the two images were quite different, and c) locations where the signal of the two images was quite different due to different scale, image quality, occlusions and shadows but mostly different reflection characteristics of the object combined with the illumination to sensor angle. This poses a question whether the selection of the tilts for the A and F cameras was really optimal (for the N hemisphere). A combination of A and Backward channel would probably lead to less radiometric differences between the stereo images and reduce saturation, while the occluded areas would be mostly to the north of 3D above-ground objects, where anyway shadows would exist. Another design possibility would be to use 2 cameras symmetric to the nadir, reducing the scale difference and image quality difference between the stereo images.

For all datasets, the quantitative evaluation was performed after first co-registering the matching and the reference DSMs by using the method described in Gruen and Akca (2005) and the respective program LS3D. Although LS3D generally uses a 7-parameter similarity transformation, in this case only 3 shifts were used, as there were no obvious rotations or scale difference between the 2 DSMs. The co-registration removes possible offsets between the two datasets (e.g. the height datum difference in the Rome datasets). In the co-registration, a robust filtering removes gross errors larger than 10 sigma, so that they do not influence the estimation of the 3 shifts (these points however are used in the computation of differences between the two DSMs). After co-registration, the Euclidian distances (E) between the two DSMs are computed pointwise, and the error is splitted in X, Y, Z components. The Mausanne reference DSM was too large (about 120 million points) and could not be treated by LS3D. Thus, two versions were examined. One with the original 2m grid spacing for a sub-area (about 35 million points), and one with a 4m subsampled DSM (by using only every second grid point) in the whole area, called MAU1 and MAU2 respectively. Due to lack of time, we did not make an analysis of the relation of the errors to terrain relief or landcover, as done in Kay and Zielinski (2006). The results for Rome_New were, against expectations, very slightly worse than the results of Rome_Old and are shown in Table 6. The large Z-shift value of 48m, is due to the difference between WGS84 related matching heights and orthometric heights of the reference DSM. Results from Mausanne are shown in the same table. As with the sensor orientation, the Mausanne results were better. The residuals smaller than -3 sigma and larger than +3 sigma were very few, namely for Rome_New 0.8% and 1.7%, MAU1 0.7% and 0.8% and MAU2 0.6% and 1.2%. The larger errors in Rome_New are partly due to errors in the reference DSM. At one of its borders large negative values up to -114 m were observed. Also the Mausanne 4m subsampled reference DSM had up to -5 m negative heights, indicating possible errors. The results for all datasets are partly influenced by the time difference between acquisition of the Cartosat-1 images and the images used for the generation of the reference DSMs.

Fig. 5 shows a visualisation of the matching DSM in Mausanne. The large rectangle shows the area of the reference DSM, the smaller one shows the subarea that was used for the comparison with the full resolution reference DSM (dataset MAU1). At the borders, on the right and lower part, large errors are visible. This happens often with Sat-PP and other matching programs. Fig. 6 shows a visualisation of the residuals of the Z-component of the Euclidean distances for MAU1. It is obvious that certain regions, due to their texture (e.g. repetitive patterns in agricultural fields), have more matching problems. Fig. 7 shows the same for the Rome_New dataset. The red color at the roads

shows that the matching DSM is higher, because matching for this ground resolution mainly uses edge information from the surrounding building roofs to find corresponding points. This is also verified by a histogram of the residuals showing that large errors are more positive than negative. Fig.8 shows a part of the Rome_Old and Rome_New matching DSMs. The first one was generated using modified cross-correlation, the second one adding at the final stage LSM. The figure shows for Rome_Old systematic errors due to low texture, poor image quality and differences between A and F, which to a large extent have been removed by using LSM.

Table 6. Statistical values of the Euclidean distances between reference and matching DSMs and values of the shift parameters (T) between the two DSMs.

Dataset	**Reference DSM points** **Matching DSM points** **No. of used points**	**Sigma-E (m)** **Sigma-X (m)** **Sigma-Y (m)** **Sigma-Z (m)**	**Mean / Min / Max - E (m)** **Mean / Min / Max - X (m)** **Mean / Min / Max - Y (m)** **Mean / Min / Max - Z (m)**	**Tx / Ty / Tz (m)**
Rome_New	33,480,832 4,013,922 25,532,034	6.81 1.35 1.32 6.54	0.06 / -41.51 / 161.22 0.00 / -30.57 / 23.19 0.00 / -27.52 / 41.17 0.01 / -40.99 / 158.45	1.34 / 3.24 / -48.43
MAU2	23,300,000 9,974,835 22,089,194	3.13 0.69 0.79 2.94	0.04 / -81.68 / 78.65 0.00 / -56.40 / 57.08 0.00 / -60.02 / 66.37 0.02 / -80.49 / 67.50	3.45 / -2.32 / 0.34
MAU1	37,506,250 9,974,835 37,494,000	2.86 0.56 0.63 2.73	0.02 / -54.47 / 43.70 0.00 / -34.68 / 33.18 0.00 / -31.77 / 35.04 0.01 / -53.98 / 42.21	3.19 / -2.91 / 0.34

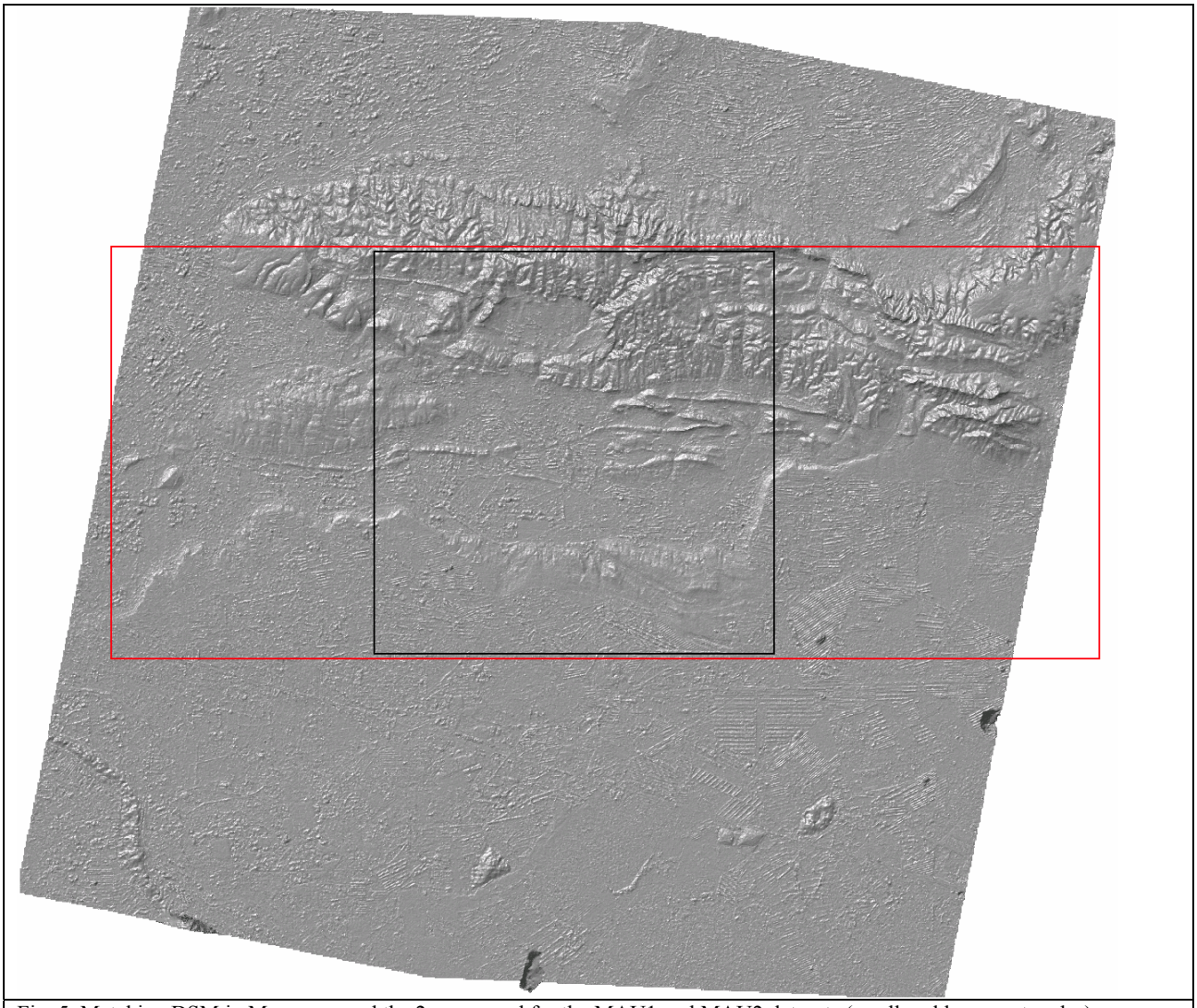

Fig. 5. Matching DSM in Mausanne and the 2 areas used for the MAU1 and MAU2 datasets (small and large rectangles).

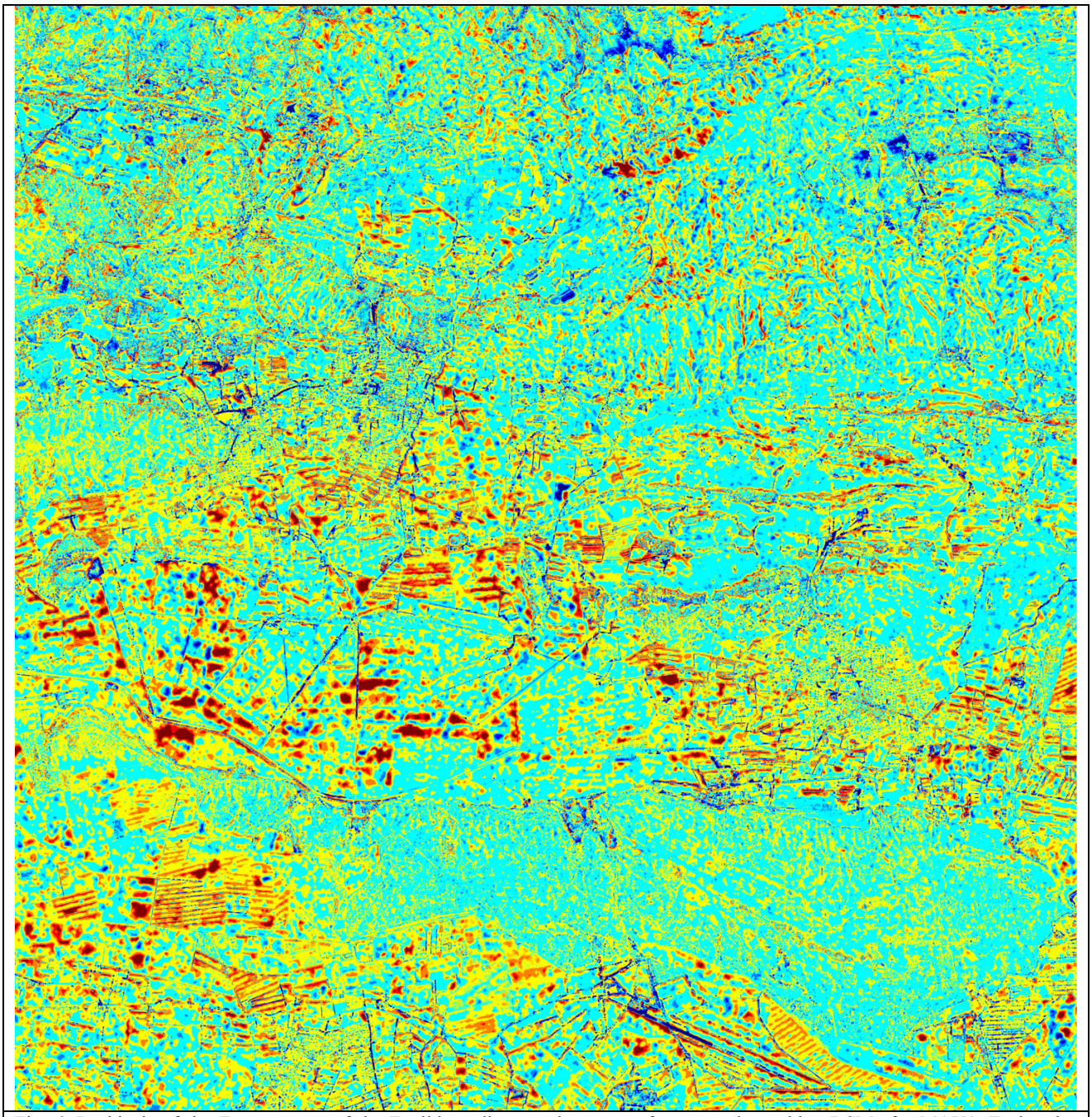

Fig. 6. Residuals of the Z-component of the Euclidean distances between reference and matching DSMs for MAU1. Each color represents one sigma (here about 3m). Light to dark blue show progressively residuals from 0 to -3 m, -3 to -6 m etc. Light yellow to red show the same but for positive residuals.

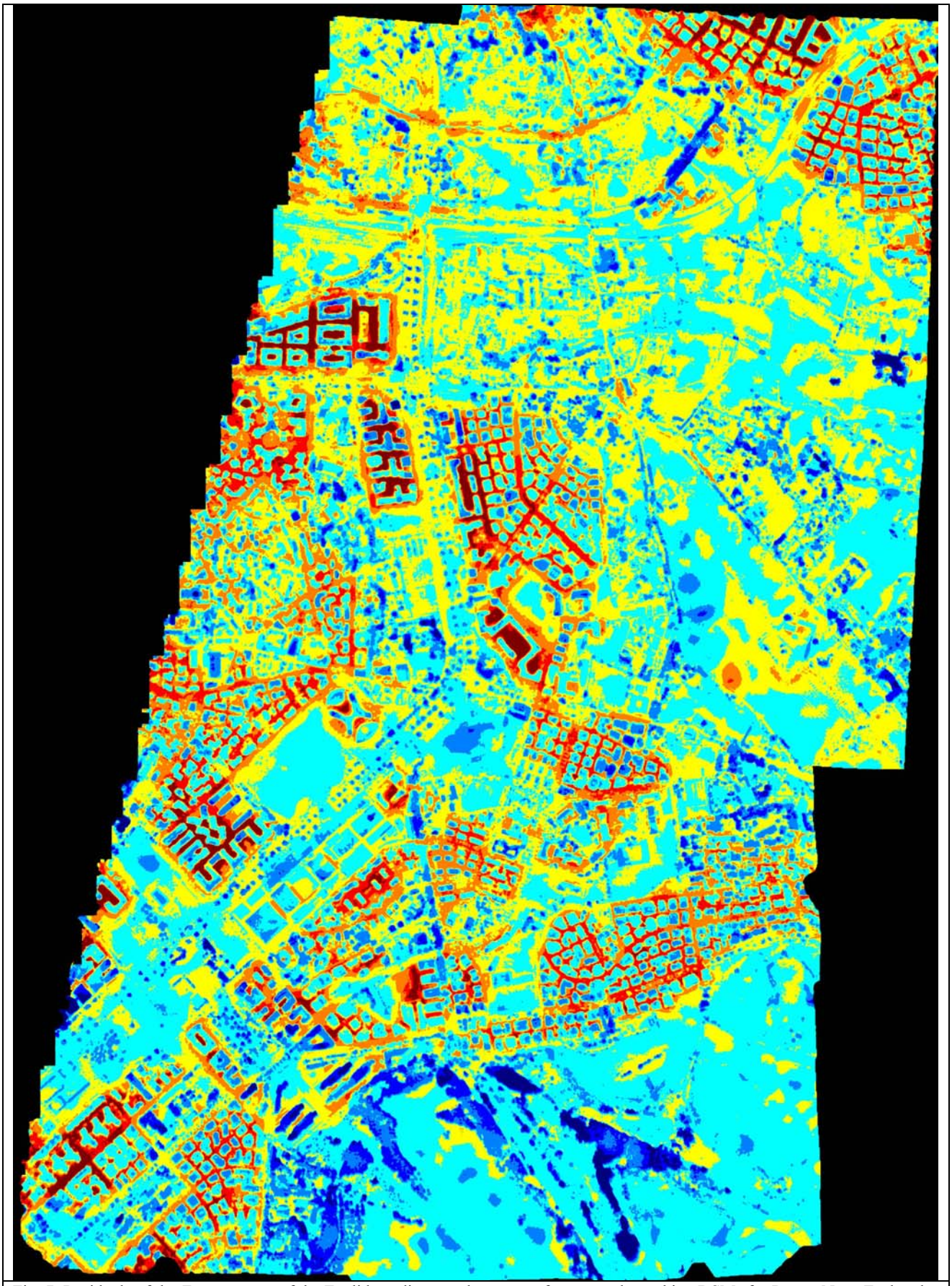

Fig. 7. Residuals of the Z-component of the Euclidean distances between reference and matching DSMs for Rome_New. Each color represents one sigma (here about 7m). Light to dark blue show progressively residuals from 0 to -7 m, -7 to -14 m etc. Light yellow to red show the same but for positive residuals.

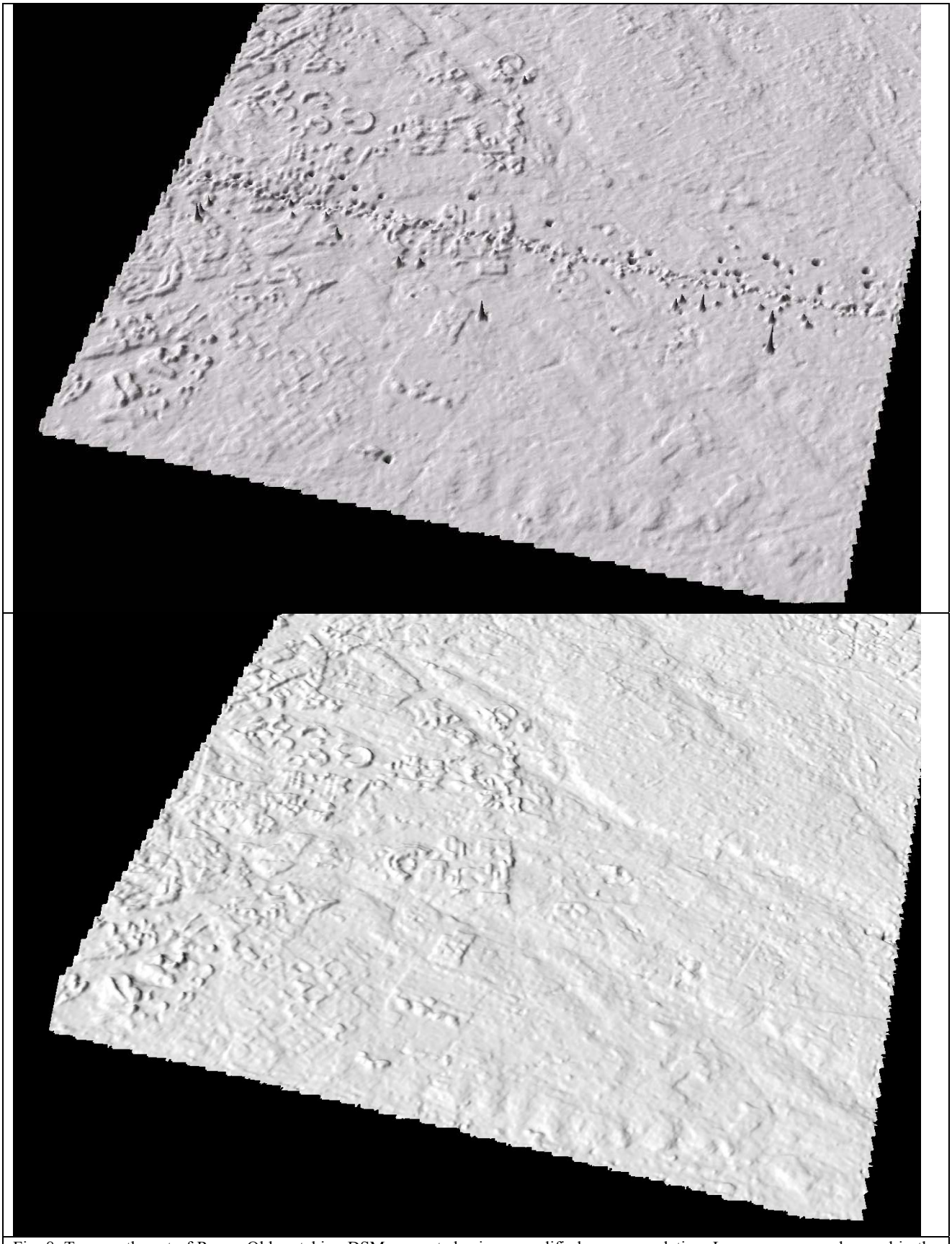

Fig. 8. Top: south part of Rome_Old matching DSM generated using a modified cross-correlation. Large errors are observed in the middle from West to East. Bottom: the same area of Rome_New matching DSM using in the final matching stage LSM. Most blunders have been removed.

6. DISCUSSION AND CONCLUSIONS

The whole C-SAP test showed various deficiencies, especially if one compares it to a previous similar activity of ISPRS with CNES regarding Spot-5. The main problem was that most test sites, at least until October 2006, had not reference data (GCPs and/or DSM) of a sufficient quality and sometimes also extent. Many of these test sites should not have been accepted by the C-SAP team. The delivered RPCs had the above mentioned problem of zero crossings. Certain aspects of imaging and image generation that may influence both geometric integrity and image quality like possible yaw and pitch steering during imaging or the method of assembling the image from the two staggered linear CCDs remain mostly unknown, as with most other providers of high-resolution satellite images who are secretive.

Regarding image quality, Cartosat-1 is better than ALOS/PRISM but inferior to Spot-5 HRS or HRG. The images exhibit pattern and interlace noise, unsharpness and horizontal edge jitter (especially in the F image). The two images, in spite of the quasi-simultaneous image acquisition, show often radiometric differences that lead to measurement errors. This is probably partly due to the unfavourable choice of viewing angles for the A and F channels, which also leads to scale differences between the images, causing again errors in matching.

Regarding the necessary sensor modelling and the accuracy potential for 3D point measurement, the following can be concluded. RPCs should be corrected by an affine transformation, shifts only do not suffice. With shifts only, systematic residuals remain, especially ones that are influenced by scale across track. The generation of the RPCs by the providers of high-resolution satellite images differs and this seems to be a little discussed but however important topic, which affects geometric accuracy and stability. Even with the new RPCs, without zero crossings, the shifts with or without affine terms are large, showing that the absolute geolocation accuracy of Cartosat-1 without GCPs is poor and by far worse than the specifications, while the geolocation accuracy varies a lot from dataset to dataset. As with other high-resolution satellite sensors, the GCPs should be well measurable in the images. Their distribution, although for many high resolution satellite sensors (e.g. Ikonos), is not so important, for Cartosat-1 seems to have a significant influence on the accuracy. Thus, to be on the safe side, a good GCP distribution is recommended. The number of the GCPs is not so crucial. For an affine correction of the RPCs and a certain redundancy, we recommend the use of about 6 GCPs as minimum. Accurate point transfer from the A to the F channel by accurate image matching (e.g. LSM) is strongly encouraged and increases the height accuracy. The planimetric accuracy achieved in the best test site (Mausanne), espec. in Northing, falls short of the accuracy that has been achieved with other satellite sensors, that was about 0.3 pixels. This can be due to the poor identification of the GCPs in the images, but also due to deficiencies in image quality and geometric stability during imaging. The height accuracy in pixels, at least in Mausanne, was exceptionally good, in spite of the suboptimal B/H ratio, even exceeding previous results achieved with sensors like Ikonos. This indicates that the errors in the planimetric positioning are rather due to the poor identification of the GCPs.

The DSM accuracy in Mausanne, the test site with a large and accurate reference DSM, was slightly over 1 pixel, for the whole area which included variable terrain relief and landcover, without any manual editing and in spite of the suboptimal B/H ratio and the significant time and epoch difference between reference DSM and matching DSM. This shows that Cartosat-1 has a good potential for generation of DSMs with a grid spacing of about 10 m and an accuracy (RMS) of about 3 m. However, this can be achieved only by using GCPs (modest in number, but well measurable). The absolute geolocation accuracy is quite poor, thus Cartosat_1 is not suitable for generation of global DSMs. All in all, in spite of some deficiencies and possible improvements, Cartosat-1 is a useful image source for 3D mapping and DSM generation.

ACKNOWLEDGEMENTS

We would like to acknowledge ISRO, India for co-organising this test and providing the image data, JRC (S. Kay and R. Zielinski) for providing the reference data of the Mausanne test site, and L. De Vendictis (Università di Roma “La Sapienza”) for providing the reference data of the Rome test site.

REFERENCES

Baltsavias, E., Zhang, L., Eisenbeiss, H., 2006. DSM Generation and Interior Orientation Determination of IKONOS Images Using a Testfield in Switzerland. Photogrammetrie, Fernerkundung, Geoinformation, (1), pp. 41-54.

Crespi, M., Barbato, F., De Vendictis, L., Onori, R., Poli, D.,, Volpe, F. , Wang, X., 2006. Orientation, orthorectification, DSM extraction and 3D city modeling by Cartosat-1 stereo imagery: first results of a test over Rome. In: International Archives of Photogrammetry, Remote Sensing and Spatial Information Sciences, Vol. 36, Part 4, on CD-ROM.

EOPortal, 2007. http://directory.eoportal.org/pres_IRSP5IndianRemoteSensingSatelliteP5CartoSat1.html (accessed 7 May, 2007).

Gruen, A., Akca, D., 2005. Least squares 3D surface and curve matching. ISPRS Journal of Photogrammetry and Remote Sensing, 59(3), pp. 151-174.

Jakobsen, K., 2006. Technical report – test area Mausanne and Warsaw. In: International Archives of Photogrammetry, Remote Sensing and Spatial Information Sciences, Vol. 36, Part 4, on CD-ROM.

Kay, S., Zielinski, R., 2006. Orthorectification and geometric quality assessment of Cartosat-1 for common agricultural policy monitoring. In: International Archives of Photogrammetry, Remote Sensing and Spatial Information Sciences, Vol. 36, Part 4, on CD-ROM.

Krishnaswamy, M., 2002. Sensors and Platforms for High Resolution Imaging for Large Scale Mapping Applications - Indian Scenario. Indian Cartographer, DAPI-01, URL: http://www.incaindia.org/technicalpapers/02_DAPI01.pdf (accssed 7 May 2007).

Lehner, M., Müller, R., Reinartz, P., 2006. Stereo evaluation of Cartosat-1 data on test site 5 - first DLR results. In: International Archives of Photogrammetry, Remote Sensing and Spatial Information Sciences, Vol. 36, Part 4, on CD-ROM.

Lutes, J., 2006. First impressions of Cartosat-1. Proc. of the Fifth Annual Joint Agency Commercial Imagery Evaluation

(JACIE) Workshop “Civil Commercial Imagery Evaluation”, 14-16 March, Laurel, MD, USA, on CD-ROM.

Poli, D., Zhang, L., Gruen, A., 2004. SPOT-5/HRS stereo images orientation and automated DSM generation. In: International Archives of Photogrammetry, Remote Sensing and Spatial Information Sciences, Vol. 35, Part B1, pp. 421-432.

Sadasiva Rao, B., Murali Mohan, A.S.R.K.V., Kalyanaraman, K., Radhakrishnan, K., 2006. Evaluation of Cartosat-I Stereo Data of Rome. In: International Archives of Photogrammetry, Remote Sensing and Spatial Information Sciences, Vol. 36, Part 4, on CD-ROM.

Spruyt, P., Kay, S., 2004. Quality assessment test with Leica Geosystems ADS40: Digital Airborne Orthoimagery. GIM International, 18(6), pp. 35-37.

Wolff, K., Gruen, A., 2007. DSM generation from early ALOS/PRISM data using SAT-PP. Proc. of ISPRS Hannover Workshop 2007 “High-Resolution Earth Imaging for Geospatial Information”, Hannover, Germany, May 29 – June 1. On CD-ROM.

Zhang, L., 2005. Automatic Digital Surface Model (DSM) Generation from Linear Array Images. Ph.D. Dissertation, Report No. 88, Institute of Geodesy and Photogrammetry, ETH Zurich. Available at http://e-collection.ethbib.ethz.ch/ecol-pool/diss/fulltext/eth16078.pdf.